# Deep UV LED research moving performance beyond 10% efficiency

**Mike Cooke reports on progress made by a number of research teams.**

Deep ultraviolet light-emitting diodes are being developed for spectral analysis, photocatalysis, air and water decontamination, and material sterilization applications. More specific uses could include biological agent detection, phototherapy, optical data storage, and photolithography.

Present DUV systems involve bulky, fragile and poisonous mercury lamps. A solid-state solution based on aluminium gallium nitride (AlGaN) LEDs is desired but for the shorter UV wavelengths external quantum efficiencies plummet to less than 12% at 20mA injection current in the range 270–280nm. For the ~250nm wavelengths needed for effective killing of bacteria and viruses, the efficiency level is a measly 3%.

The poor performance is attributed to a number of factors. For example, the magnesium doping used to achieve p-AlGaN has activation energies (500–600meV) even higher than that of p-GaN (~180meV), which is already a poor performer in long wavelength LEDs. High activation energy means low carrier concentrations and hence low conductivity.

A further obstacle in DUV LEDs is that a thin p-GaN layer is added to achieve decent ohmic contact with the metal p-electrode. The DUV photons have sufficient energy to excite electrons from the valence band to the conduction band and hence these p-GaN layers absorb the light emitted by the active layers, cutting light extraction efficiency.

Here we look at recent research that attempts to tackle the problems of low efficiency in DUV devices.

## Beyond 10% efficiency

A team of researchers based in the USA has described two of the main developments that has allowed them to push external quantum efficiencies beyond 10% [Max Shatalov et al, Semicond. Sci. Technol., vol29, p084007, 2014]. The team is associated with Sensor Electronic Technology Inc (SETi), US Army Research Laboratory, and Rensselaer Polytechnic Institute.

The researchers comment on one aspect of their work: "Large chip LEDs with the output power >75mW CW at 300mA pave the way for DUV semiconductor sources to be used in disinfection, decontamination, curing and medical applications."

SETi is on its third generation of DUV LED, achieving about 10% external quantum efficiency (EQE) and 4.5% wall-plug efficiency (WPE) at 20mA injection in the 270–280nm wavelength range. To achieve improvement over previous generations the researchers focused on reducing the effect of non-radiative (NR) defects and decreasing optical losses in p-GaN contact layers and through the refractive index mismatch between the device material and air.

The more recent SET devices use a short-period superlattice (SPSL) of various compositions of p-AlGaN. The technology was first developed for less challenging UV-A (400–315nm) and UV-B (315–280nm) devices and then the Al-content was increased to cross the border into UV-C (280-100nm). Factors that can be adjusted to improve performance include reducing the SL period and tuning the well/barrier compositions to align the hole ground state in the well with the acceptor level in the barrier.

At 275nm, the normal incidence optical transmission can be increased to more than 60% for a p-SPSL, compared with 5% for p-GaN contact layers. Unfortunately, the higher activation energy of the Mg acceptors in AlGaN leads to a higher operating voltage that decreases WPE at high current in small area devices.

SETi has also developed metal stack reflectors on the p-contact in its Gen II devices with 70% normal incidence reflectivity in the UV region. The researchers attribute an improvement of nearly a factor of two in light extraction efficiency (LEE) and EQE to the use of a metal reflector.

Reduced threading dislocation density (TDD) has been achieved through the application of migration-enhanced metal-organic chemical vapor deposition (MEMOCVD) on sapphire with AlN buffer layers. MEMOCVD heterostructures with AlGaN/AlN superlattice transition layers between the buffer and device layers have cut TDD from $5x10^9/cm^2$ (Gen I/II) to $2x10^8/cm^2$ (Gen III). The transition layer minimizes relaxation and avoids cracking of AlGaN layers grown over AlN templates.

The researchers believe further improvements in material quality can be achieved through growth parameter optimization to alter point defect concentration, quantum well interface sharpness, and alloy composition uniformity.

The use of low-TDD AlN templates ($2x10^8/cm^2$) allowed the researchers to achieve EQE values of more than 10% in Gen III devices (Structure B, Figure 1). This doubles the EQE of 5% achieved with Gen II devices using higher TDD templates ($3–5x10^9/cm^2$) along with LEE enhancements such as surface roughening and encapsulation (Structure A). An intermediate $5x10^8/cm^2$ TDD large-area device (Structure C) suffered from LEE problems due to optical losses in the p-SPSL contact region and absorption by n-contacts.

The lower-TDD structures B and C also exhibited earlier onset of efficiency droop at ~$5A/cm^2$ current density, compared with ~$50A/cm^2$ for structure A. The researchers suggest that the efficiency droop could be due to delocalization of free carriers at higher current densities. With higher defect densities the carriers can be bound to certain regions, inhibiting their migration to non-radiative recombination centers, delaying efficiency droop.

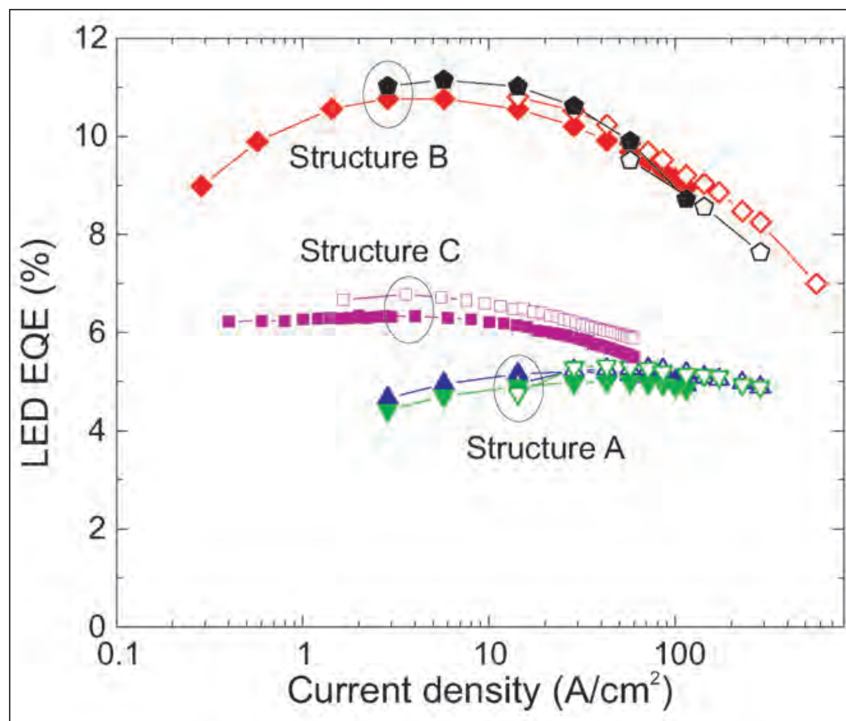


**Figure 1. EQE versus current density of LED devices from structures A, B and C under CW (closed symbols) and pulsed (open symbols) pumping.**

The large area device based on Structure C achieved continuous wave (CW) 275nm wavelength output powers of 27mW and 75mW at 100mA and 300mA, respectively. The corresponding EQEs were 6% and 5.5%. Using pulsed operation to avoid self-heating effects increased the output power at 300mA to 80mW. At 100mA current, the forward voltage was less than 7V, giving an electrical efficiency of ~60%.

The researchers comment: "It is evident that, for the large chip devices, use of SPSL top layer is more beneficial since the p-contact and the p-layer voltage drop contribution into the operating voltage is not as strong as in small chip devices."

## Nanopipes and light extraction

The USA-based Sandia National Laboratories has recently published two papers on DUV light emitting structures that deal with different challenges for increasing efficiency.

In the first piece of work, the team sought to find ways to characterize and thus reduce performance-killing defects, in particular open-core threading dislocations or 'nano-pipes' with diameters between 2nm and 50nm [Michael Moseley et al, J. Appl. Phys., vol116, p053104, 2014].

The researchers prepared a pair of silicon-doped $Al_{0.7}Ga_{0.3}N$ templates on sapphire, using a Veeco MOCVD system. One of the templates was used for defect analysis, the other for fabricating LEDs (Figure 2). The template layer was grown on a 3.75µm AlN buffer. X-ray diffraction analysis determined that the total

| Contact | p-GaN | 150nm |
|---|---|---|
| Electron blocking | p-$Al_{0.9}Ga_{0.1}N$ | |
| MQW | 3x($Al_{0.44}Ga_{0.56}N$/ $Al_{0.55}Ga_{0.45}N$) | 3x(2.6nm/4.3nm) |
| Contact | n-$Al_{0.65}Ga_{0.35}N$ | 500nm |
| Template | $Al_{0.7}Ga_{0.3}N$ | 1.3µm |
| Buffer | AlN | 3.75µm |
| Substrate | Sapphire | |

**Figure 2. Epitaxial structure of Sandia LEDs.**

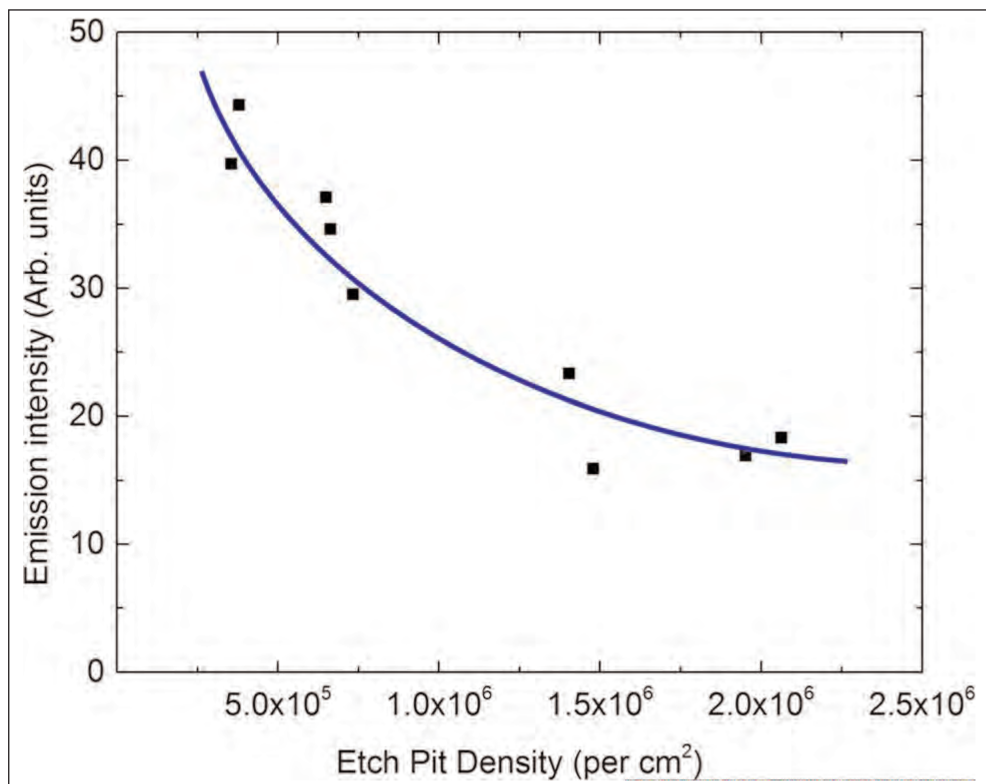


**Figure 3. Relative output powers of LEDs grown on AlGaN template versus micron-scale etch pit densities at corresponding location on etched AlGaN template. Line is drawn to guide the eye.**

The researchers see these optical microscope studies of micron-scale etch pits as an efficient means to determine nano-pipe densities across wafers, in contrast to time-consuming AFM studies. Compared with the total threading dislocation density, the nano-pipe density is about four orders of magnitude lower at around $7.5x10^5/cm^2$. Variation in density across the wafer was nearly an order of magnitude, between $4x10^5/cm^2$ to $2.1x10^6/cm^2$. Variation in total threading dislocation density was only 15%.

The Sandia team adds that recent improvements in nitridation, nucleation, and buffer growth have reduced the density of nano-pipes by almost two orders of magnitude, with etch pits providing a "crucial feedback" for process optimization.

Closed-core threading dislocations give nanometer-scale etch pits after exposure to 160° phosphoric acid for 30 seconds that can be detected using tapping-mode AFM.

threading dislocation density was $2–2.4x10^9/cm^2$.

Before defect analysis, a further unintentionally doped 1μm AlGaN layer was grown. The analysis consisted of various atomic force microscope (AFM) scans and microscopic and AFM study of phosphoric acid etch-pits.

Among the scans, the researchers used conductive AFM (CAFM) in contact-mode to probe current leakage structures. It was found that repeatedly scanning for leakage had an unintended passivation effect whereby the current detected was reduced with each scan. Therefore multiple scanning would underestimate leakage.

Phosphoric acid etching at 160°C for 60 seconds was used to distinguish nano-pipes. The reactants enter the pipes, dissolving material and creating 1–2μm-wide hexagonal pits. Such defects have been associated with current leakage. The growth mechanism of nano-pipes is unclear, but seems to be correlated with impurities such as silicon, magnesium and oxygen. The electrical conduction is thought to be along the walls of the pipes with the impurities creating a current path.

Comparing the etch pits with the CAFM measurements, the researchers found micron-scale etch-pits at the sites of current leakage. The team comments: "Based on the similarity in etch behavior to previous reports of nanopipe decoration in concert with the detection of current transport at these sites of hexagonal etch pits, we conclude that the source of these etch pits are open-core threading dislocations."

(The tapping mode allows finer features to be resolved.) The density of the nano-scale etch pits was estimated at $2.5x10^9/cm^2$. There was found to be little variation in nano-scale etch pit density across the sample.

Having mapped out the nano-pipe density for different parts of the wafer, the researchers set out to find correlations with the performance of LEDs produced on the second sample. Previous work had convinced the team that such correlations were meaningful: "The distribution of etch pits was previously found to be similar across multiple templates produced in the same growth run."

The LEDs measured 300μm x 300μm. The emission wavelength was 270nm. The researchers found an inverse proportionality relation between relative output power and assumed micron-scale etch pit density (Figure 3). No such correlation was found between total threading dislocations and micron-scale etch pits.

The researchers comment: "This strong correlation between LED performance and micron-scale hexagonal etch pits is attributed to the electrical current leakage associated with the open-core threading dislocations. These current transport paths can shunt the quantum well active regions by carrying current directly across the junction without the opportunity to radiatively recombine."

The team therefore concludes: "These data suggest that nanopipes acting as current leakage paths can have a larger effect on LED electroluminescence than

threading dislocations acting as non-radiative recombination centers."

In the second report, the team studied the use of scattering structures to overcome poor light extraction from DUV LEDs [J. J. Wierer Jr., et al, Appl. Phys. Lett., vol105, p061106, 2014].

The epitaxial structures were produced by metal-organic vapor phase epitaxy (MOVPE) on sapphire (Figure 4). The multiple quantum well (MQW) active region consisted of the three periods of $Al_{0.44}Ga_{0.56}N$ in $Al_{0.55}Ga_{0.45}N$ barriers. The nominal well and barrier thicknesses were 2.6nm and 2.9nm, respectively, but the actual parameters varied across the epitaxial wafer. The electroluminescence peak was at 269±2nm.

The epitaxial material was processed into flip-chip UV LEDs. The p-contact consisted of a thin layer of nickel and an aluminium mirror of 60–70% reflectivity. The effectiveness of the mirror in extracting UV from the structure tends to be negated by the absorption of radiation by the relatively narrow bandgap (3.4eV, 365nm wavelength) of the p-GaN contact layer.

The scattering structures were created by etching down through the QWs to the n-contact layer. The n-contact regions were also formed at the same time. The scattering structures consisted of 5μm trenches with 70–80° sidewalls, giving hexagonal or triangular arrays. The trenches were filled with 200nm of silicon dioxide and then 200nm of aluminium. The silicon dioxide electrically isolated the trenches. The aluminium acted as both mirror and electrical connection between the isolated hexagonal or triangular areas.

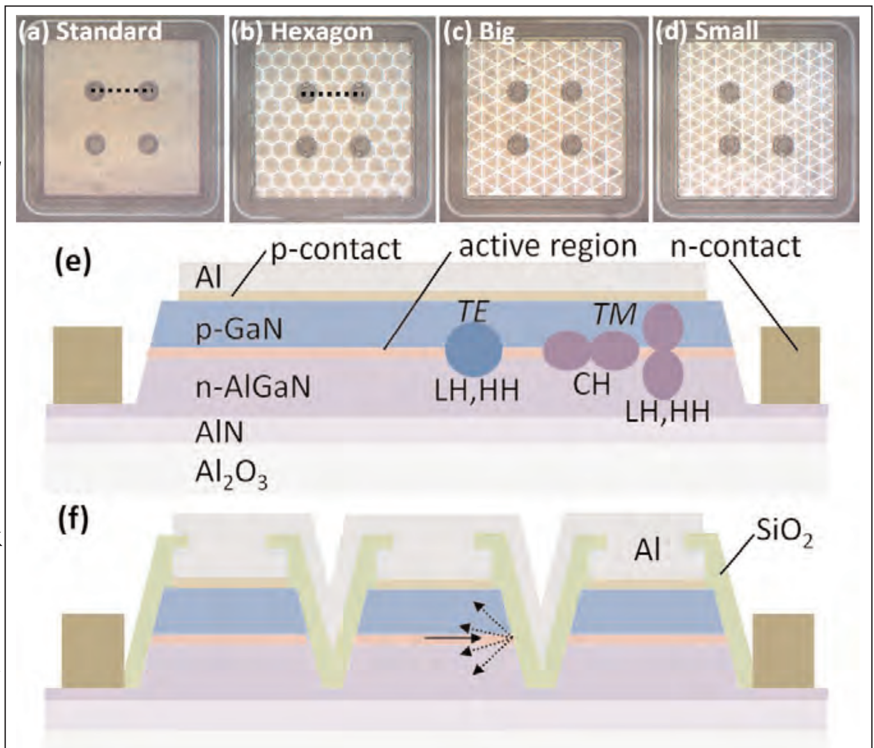


**Figure 4. Optical microscope images through sapphire substrate of (a) standard, and (b) hexagonal, (c) big triangle, and (d) small triangle reflective scattering structure UVLEDs. Cross-section schematic of standard UVLED (e) showing emission patterns of TE and TM polarized light for transitions to light- and heavy-hole subbands (LH and HH, respectively) and to crystal field split-off hole subbands (CH). Cross-section schematic of UVLEDs with reflective scattering structures (f) showing scattering of in-plane light (arrows) from reflective scattering structure. Dashed lines in (a) and (b) are positions of cross-sections in (e) and (f).**

The n-contact was formed by 20μm-diameter circular regions and a 20μm trace around the periphery of the device. The n-contacts were connected over the p-contact with silicon dioxide insulation and gold-based connecting and bonding metal.

The sapphire substrate, through which the light was designed to be emitted, was thinned to 250μm. The wafer was singulated into 1mmx1mm chips containing 2x2 arrays of UV LEDs. The devices were not packaged. One edge of the devices was polished to facilitate optical polarization measurements.

The effectiveness of the scattering structures was greatest when there was the largest fraction of light trapped in the plane of the LEDs. In fact, the in-plane radiation was greatest when the optical polarization of the radiation was least (Figure 5). This effect was related to details of the band structure that varied with QW thickness, etc. In longer wavelength InGaN QWs the light tends to be polarized parallel to the plane, favoring perpendicular emission into the light escape cone. For AlGaN QWs the light is polarized both perpendicular and parallel to the QW plane, resulting in more trapped light.

## Nonpolar substrates

Researchers at NTT Corporation, Japan, have used nonpolar m-plane substrates to find ways to overcome the problem of optical polarization [Ryan G. Banal et al, Appl. Phys. Lett., vol105, p053104, 2014]. The team studied 4-period, 1nm to 4nm $Al_{0.56}Ga_{0.44}N$ MQWs in 6nm $Al_{0.88}Ga_{0.12}N$ barriers produced by MOVPE on c- and m-plane AlN bulk substrates. The epitaxial samples were produced under identical process conditions in the same run.

The m-plane MQWs were found to have undulations that "occurred during the MOVPE growth because of the formation of macrosteps on the surface, which could be suppressed by using appropriate growth conditions and off-cut angles of the substrate surface," according to the NTT team.

Photoluminescence at 9K showed peaks at 237.7nm

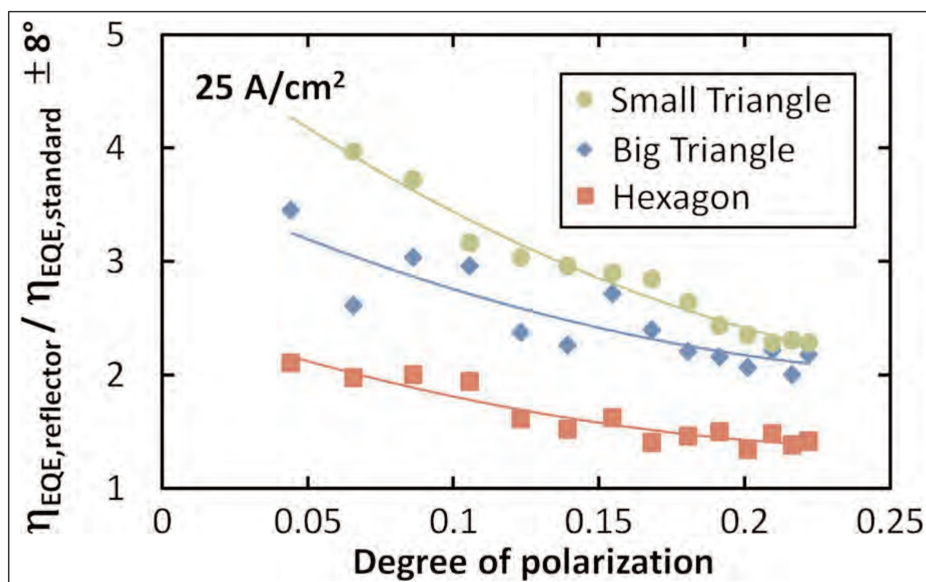


**Figure 5. Ratio of EQE in ±8° collection cone of reflective scattering and standard UVLEDs versus degree of polarization at 25A/cm².**

— an effect mainly attributed to the quantum-confined Stark effect (QCSE), which is not present in the m-plane samples.

Optical polarization measurements showed that the radiation with electric field parallel ($E_{||c}$) to the c-direction was stronger than that in the perpendicular direction ($E_{\perp c}$). The m-plane 4nm-well sample was more strongly polarized at –0.91, compared with –0.58 for the c-plane MQW structure. (Positive optical polarization indicates when perpendicular electric fields predominate. Negative polarization shows parallel fields.) Over the range of well widths, the m-plane polarization remains parallel, but the c-plane sample crosses over to perpendicular polarization for the narrowest wells (Figure 7).

(5.216eV) and 249.8nm (4.963eV) for 4nm m- and c-plane wells, respectively. The c-plane sample also has a larger linewidth of 7.63nm (150meV), compared with 5.13nm (112meV) for m-plane MQWs. The researchers attribute this to a shoulder in the c-plane spectrum due to multiple factors such as a phonon replica peak and compositional inhomogeneity. At room temperature, the linewidths were 6.08nm (132meV) and 9.54nm (188meV) for the m- and c-plane MQWs, respectively.

Over the range of 1-4nm well widths, both samples showed decreasing photon energy (increasing wavelength) as the well width increased (Figure 6). At all widths, the c-plane sample emitted lower energy photons

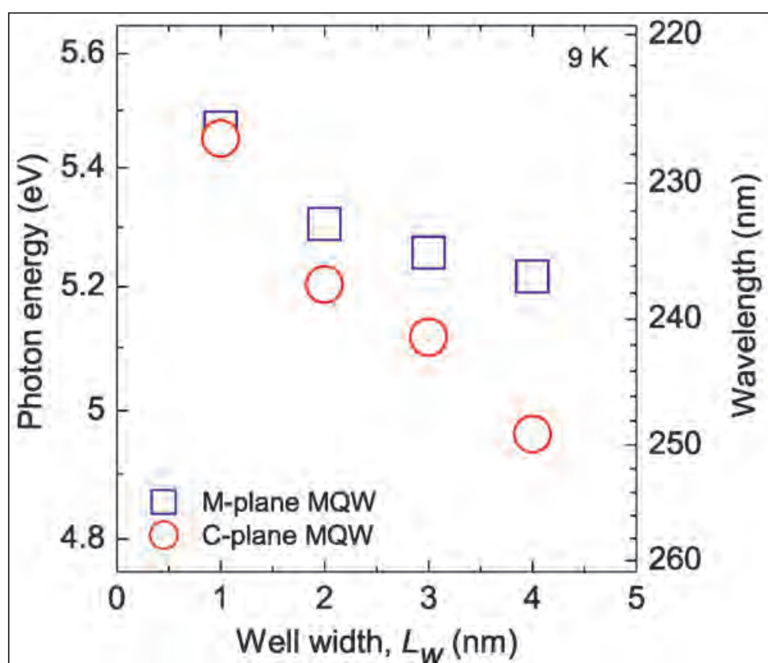


**Figure 6. Peak emission energy (emission wavelength) of m- and c-plane AlGaN MQWs versus well width at 9K.**

The researchers comment: "The strong $E_{||c}$ polarization along with the absence of the QCSE in the nonpolar AlGaN MQW structures will make them a promising approach for increasing the emission efficiency of AlGaN deep-UV LEDs."

## Boron nitride p-contacts

Professors Hongxing Jiang and Jingyu Lin at Texas Tech University believe that using boron nitride as the p-type contact layers in nitride semiconductor heterostructures "could ultimately pave the way toward the realization of high efficiency nitride deep ultraviolet (DUV) optoelectronic devices" [Semicond. Sci. Technol., vol29, p084003, 2014].

Jiang and Lin see the most important roadblock for DUV applications as being the poor p-type hole carrier densities and conductivity of AlGaN at the high aluminium fractions needed for short wavelengths.

Jiang and Lin have been exploring the growth of boron nitride in the hexagonal crystal structure (hBN) as an alternative to GaN. Although the lattice mismatch between hBN and wurtzite AlN is large at 19.54%, Jiang and Lin noticed that 4x the 'a' lattice constant of wAlN (4x0.3112nm = 1.245nm) is almost equal to 5x the 'a' lattice constant of hBN (5x0.2504nm = 1.252nm). The researchers comment: "This 5/4 coincidence in the hBN/w-AlN heterojunction interface reduces the effective lattice-mismatch from 19.54% to about 0.58%."

Texas Tech has not as yet reported a DUV LED with h-BN p-contact layer, but pn diodes with "decent" behavior have been demonstrated. Jiang and Lin hope use of p-hBN contact layers in DUV LEDs (Figure 8) will enhance hole injection efficiency, more effectively block electrons from entering the p-contact region, reduce contact resistance and dramatically increase

UV transparency for wavelengths longer than 230nm due to the wide ~6eV bandgap of hBN.

The p-hBN/n-AlGaN diode heterostructures were grown using MOCVD on sapphire substrates. The p-BN layer used tri-ethyl boron, ammonia and bis-cyclopentadienyl-magnesium as precursors.

A low-temperature 800°C buffer layer was used to avoid adhesion problems and cracking. The quality of the p-hBN epilayer improved as the buffer was thinned from 140nm to 20nm.

The growth temperature of the hBN epilayer was in the range 1300–1350°C. The hBN layer had an x-ray diffraction (002) rocking curve full-width at half-maximum of 662arcsec — larger than for hBN grown directly on sapphire. This indicates room for improvement in crystal quality.

The p-hBN was activated with a 1150°C anneal for 45 minutes in nitrogen. When grown on an insulating substrate the p-hBN epilayer has demonstrated a 2.3Ω-cm resistivity. The researchers estimate the activation energy at 31meV based on temperature dependent resistivity measurements.

The present p-hBN epilayers have low mobility (~$2cm^2$/V-s) and free hole concentrations lower than expected (~$10^{18}/cm^3$ when doped with magnesium concentration of $10^{19}/cm^3$). The researchers believe that appreciable concentrations of defects may be acting as free hole compensating centers. The source of the defects is presently unclear. Clarification should lead to larger carrier concentrations and higher mobility.

The pn diode was achieved with an inductively coupled plasma etch to expose the n-type AlGaN layer. The n-contact metals consisted of annealed titanium/aluminium/nickel/gold. The p-contact was nickel/gold. The p-contact was annealed in a variety of conditions but full characterization of the ohmic contact resistance and comparison with p-GaN remains to be performed. With 1020°C annealing of the p-hBN/metal contact, the reverse bias leakage at –10V was 3μA. ■

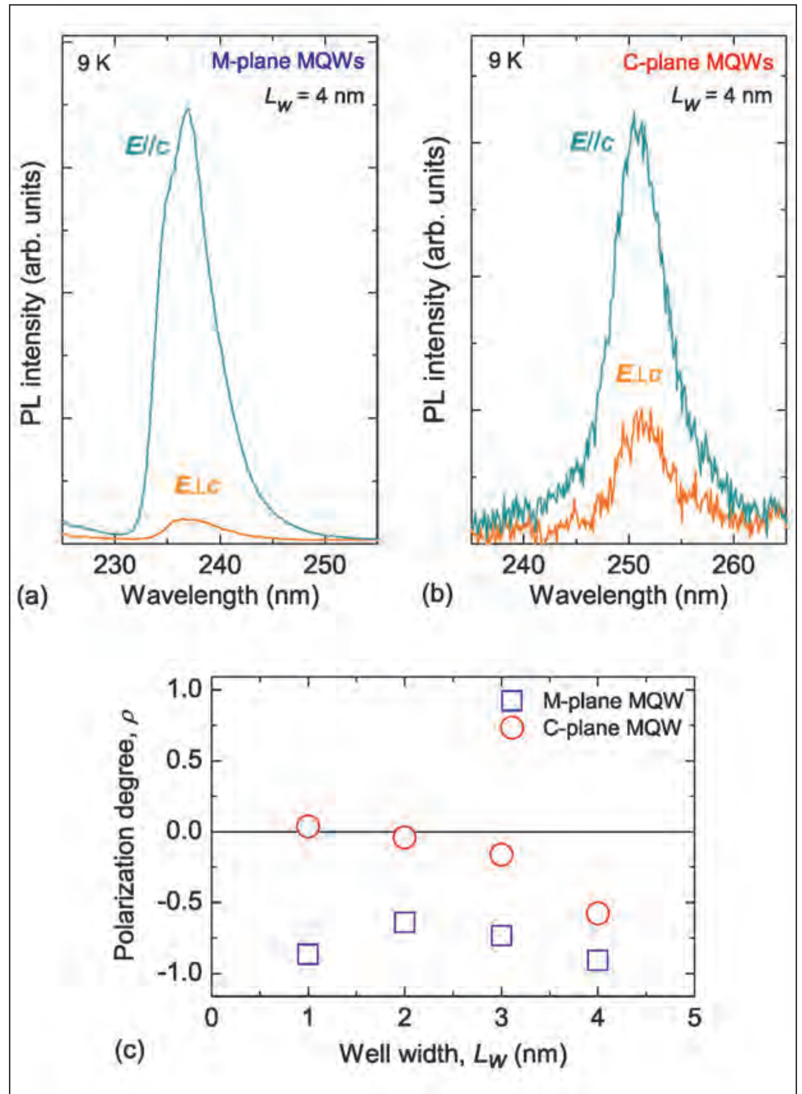


**Figure 7. Polarization photoluminescence (PL) spectra at 9K from (a) m- and (b) c-plane AlGaN MQWs with 4nm wells. (c) Polarization degree (ρ) of the PL from the m- and c-plane AlGaN MQWs as function of well width.**

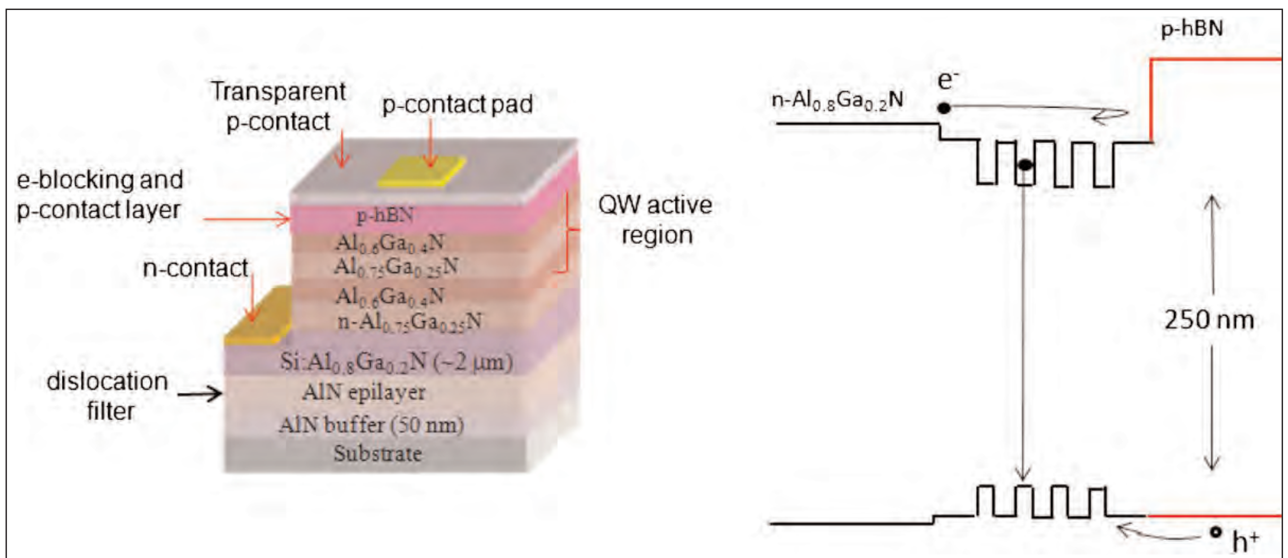


**Figure 8. (a) Schematic of DUV LED layer structure proposed by Texas Tech. (b) Energy band diagram of DUV LED layer structure suggests a band alignment that blocks electrons from entering p-contact region, while posing little barrier to holes entering active region.**